Subdiffusive Exciton Transport in Quantum Dot Solids

ARTICLE *in* NANO LETTERS · MAY 2014

Impact Factor: 13.59 · DOI: 10.1021/nl501190s · Source: PubMed

9 AUTHORS, INCLUDING:

Gleb Akselrod
Duke University
30 PUBLICATIONS **377** CITATIONS
SEE PROFILE

Ferry Prins
ETH Zurich
25 PUBLICATIONS **523** CITATIONS
SEE PROFILE

Elizabeth M Y Lee
Massachusetts Institute of Technology
6 PUBLICATIONS **25** CITATIONS
SEE PROFILE

William A Tisdale
Massachusetts Institute of Technology
21 PUBLICATIONS **686** CITATIONS
SEE PROFILE

NANO LETTERS

Letter

pubs.acs.org/NanoLett

Subdiffusive Exciton Transport in Quantum Dot Solids

Gleb M. Akselrod,[†,‡,#] Ferry Prins,[†,§,#] Lisa V. Poulikakos,[†,§] Elizabeth M. Y. Lee,[†,§] Mark C. Weidman,[†,§] A. Jolene Mork,[†,∥] Adam P. Willard,[†,∥] Vladimir Bulović,[†,⊥] and William A. Tisdale*[,†,§]

[†]Energy Frontiers Research Center for Excitonics, [‡]Department of Physics, [§]Department of Chemical Engineering, [∥]Department of Chemistry, and [⊥]Department of Electrical Engineering and Computer Science, Massachusetts Institute of Technology, Cambridge, Massachusetts 02139, United States

Supporting Information

ABSTRACT: Colloidal quantum dots (QDs) are promising materials for use in solar cells, light-emitting diodes, lasers, and photodetectors, but the mechanism and length of exciton transport in QD materials is not well understood. We use time-resolved optical microscopy to spatially visualize exciton transport in CdSe/ZnCdS core/shell QD assemblies. We find that the exciton diffusion length, which exceeds 30 nm in some cases, can be tuned by adjusting the inorganic shell thickness and organic ligand length, offering a powerful strategy for controlling exciton movement. Moreover, we show experimentally and through kinetic Monte Carlo simulations that exciton diffusion in QD solids does not occur by a random-walk process; instead, energetic disorder within the inhomogeneously broadened ensemble causes the exciton diffusivity to decrease over time. These findings reveal new insights into exciton dynamics in disordered systems and demonstrate the flexibility of QD materials for photonic and optoelectronic applications.

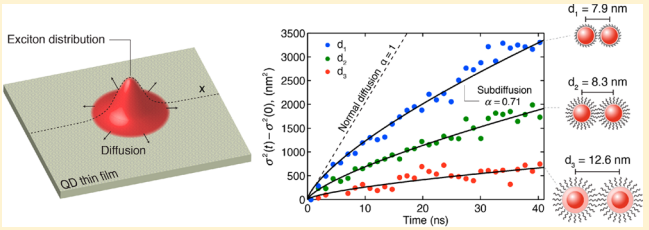

KEYWORDS: *Energy transfer, diffusion, subdiffusion, semiconductor nanocrystal, photovoltaic, LED, FRET*

Colloidal quantum dots (QDs) are semiconductor nanocrystals with size-tunable optical properties.[1] QDs are promising components of next-generation optoelectronic technologies due to solution processability,[2] narrow and size-tunable emission spectrum,[3] and the possibility for novel physics at the nanoscale that might enable enhanced power conversion efficiency.[4,5] Indeed, a number of device architectures now employ QDs as the active optical material with great success: QD-based light-emitting diodes have recently been demonstrated with external quantum efficiency close to the theoretical maximum,[6] solar cells based on QDs have obtained overall power conversion efficiencies exceeding 7%,[7] QD photodetectors have been fabricated that surpass the performance of epitaxial devices,[8,9] and lasers based on QD materials have shown tunable emission across the entire visible range.[10,11]

Central to the operation of these devices is the formation, transport, and decay of bound electron−hole pairs (excitons) and free charges. For instance, in QD solar cells the efficient diffusion of charges or excitons to charge-separating interfaces is an essential step in photocurrent generation.[2] On the other hand, exciton diffusion to quenching interfaces in QD light-emitting diodes is a process that limits luminescence efficiency.[6,12] Whether a particular material is dominated by charge carrier or exciton transport depends critically on the electronic coupling strength between neighboring quantum dots and the exciton binding energy of the material. For example, in lead-based QD solids with weak exciton binding energy and short ligands, photogenerated excitons dissociate rapidly into free charge carriers, which then move through the film by hopping or band-like transport.[13−15] On the other hand, transport in cadmium-based core−shell QD solids with strong exciton binding energy and weaker electronic coupling is dominated by Förster hopping of excitons.[16,17] While several studies have recently appeared[18−21] exploring charge carrier diffusion in colloidal QD solids, including the charge carrier diffusion length[18,21] and the role of site energy disorder,[19,20] comparatively little is known about exciton transport.

Kagan et al. first showed that the ensemble photoluminescence spectrum of a close-packed QD solid is red shifted due to resonant energy transfer within the sample inhomogeneous distribution.[16] Later, Crooker et al. used spectrally resolved transient photoluminescence to monitor downhill excitonic energy migration in the time domain.[17] More recent studies have continued to focus on the dynamics of QD energy transfer.[22−25] The distance of exciton propagation in QD solids, however, has not been explicitly studied. Furthermore, it is unclear what effect downhill energy migration has on the exciton diffusivity in inhomogeneously broadened QD assemblies and to what extent the exciton diffusion length can be tuned by surface modification.

Here, we report the direct visualization of exciton transport in colloidal QD assemblies using time-resolved optical microscopy[26] (Supporting Information). By combining direct spatial imaging experiments with measurements of spectral dynamics and kinetic Monte Carlo simulations, we reveal the

Received: March 31, 2014
Revised: April 30, 2014
Published: May 7, 2014

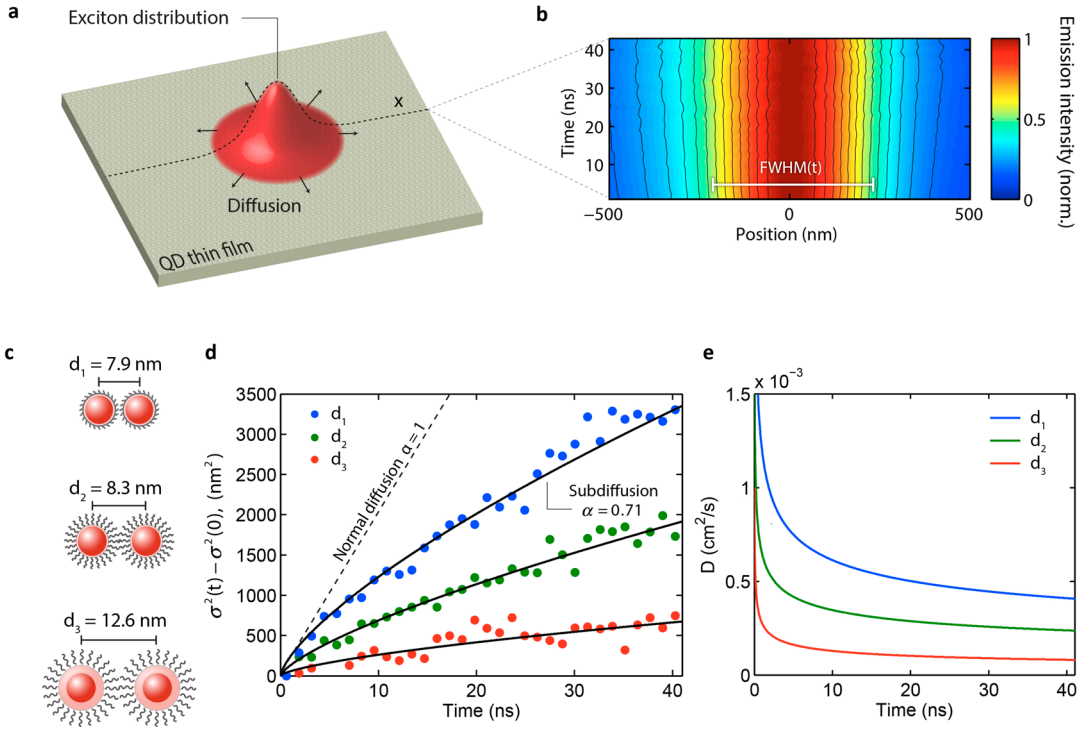

Figure 1. Imaging of exciton transport. (a) Cartoon illustrating time-dependent broadening of the exciton distribution. (b) Experimental time-evolution of the photoluminescence spatial cross-section. The peak intensity has been normalized to emphasize the time-dependent broadening of the emission profile. The linear color scale indicates normalized photoluminescence intensity. (c) Schematic representation of the three types of quantum dot samples studied, depicting the ligand and shell thicknesses used to space out the dots and indicating the center-to-center separation as determined by electron microscopy. (d) Change in variance, σ^2, of the exciton distribution as a function of time for the three samples. Solid lines are fits to a power law (see eq 2 in the main text). The dashed line represents the hypothetical case of normal diffusion in which the variance grows linearly with time. (e) Diffusivity, D, plotted as a function of time.

details of exciton transport in space, time, and energy. We show that energetic disorder, an inherent property of QD solids, results in a time-dependent diffusivity, with diffusion proceeding more slowly as excitons move energetically downhill. Furthermore, we confirm that the exciton diffusion length can be controlled by modifying the length of QD surface ligands[12,14] or the thickness of an inorganic shell, highlighting the flexibility of QD materials in photonic and optoelectronic applications.

To measure exciton transport spatially, a pulsed laser (λ = 405 nm) focused to a near-diffraction-limited spot excites an initial distribution of excitons in the plane of a ~80 nm thick QD film (see the Methods section and Supporting Information for detailed descriptions of the experimental apparatus and data analysis procedures). The initial distribution broadens in time as excitons diffuse from areas of higher exciton density to areas of lower exciton density (Figure 1a). By measuring the photoluminescence emission intensity as a function of position and time, the time-dependent exciton distribution is reconstructed. Results from one of these experiments are shown in Figure 1b. The emission intensity at time t = 0 has a full width at half-maximum (fwhm) of 481 (±2) nm, which broadens to 505 (±2) nm at t = 40 ns. Although the initial size of the exciton distribution is limited by the smallest focal spot possible with far-field optics, the large signal-to-noise ratio in our measurement makes it possible to observe even small changes (±2 nm) in the exciton distribution.[26] All measurements were performed at an incident laser fluence of 0.2 μJ/cm^2, corresponding to an excitation probability of 1 absorbed photon per 500 QDs per pulse, confirming that these experiments were conducted in the noninteracting exciton regime.

To demonstrate control of exciton transport, we compare spatially resolved measurements in three QD materials (Figure 1c). All three samples are based on CdSe cores of nearly identical size (diameter ≈ 4.2 nm, λ ≈ 600 nm, emission fwhm ≈ 25 nm) with photoluminescence quantum efficiency exceeding 80%. Samples d_1 and d_2 differ by the size of their surface-bound organic ligands; samples d_2 and d_3 differ by the thickness of the inorganic shell surrounding the CdSe core. As measured by electron microscopy (see Supporting Information Figures S2 and S3), the average center-to-center spacing in each sample is d_1 = 7.9 ± 0.9 nm, d_2 = 8.3 ± 1.0 nm, and d_3 = 12.6 ± 1.0 nm. On the basis of theoretical models,[27] we expect that each QD in our disordered three-dimensional films has 4−6 nearest neighbors and that the number of nearest neighbors does not depend on ligand length or shell thickness.

To quantitatively analyze the time-dependent broadening of the exciton distribution, we plot the change in variance σ^2 versus time for the three samples (Figure 1d). The QD assemblies with smaller center-to-center separations exhibit faster broadening of the exciton distribution. To extract the exciton diffusivity, we analyze the time rate of change of the variance. For a simple random walk, or normal diffusion, the variance grows linearly with time

$$\sigma^2(t) - \sigma^2(0) = 2Dt \quad (1)$$

where $\sigma^2(t)$ is the variance at time t, $\sigma^2(0)$ is the variance of the initial distribution created by the laser pulse, and D is the diffusivity. In all three QD samples, the variance is observed to

dx.doi.org/10.1021/nl501190s | Nano Lett. 2014, 14, 3556−3562

grow sublinearly (see Figure 1d) with faster growth observed for smaller inter-QD spacing. For sublinear growth, the change in variance can be parametrized by

$$\sigma^2(t) - \sigma^2(0) = At^{\alpha} \quad (2)$$

where A is a proportionality factor with fractional time units and α is the diffusion exponent. For $\alpha = 1$, we recover eq 1 for normal diffusion. If $\alpha < 1$, the transport is said to be subdiffusive[28] with a time-dependent diffusivity $D(t) = 1/2At^{\alpha-1}$. $D(t)$ for each of the three samples is plotted in Figure 1e. In each case, rapid initial diffusion is followed by an approach toward a slower, quasi-static diffusivity.

Subdiffusive transport can result from asymmetric site-to-site hopping rates in a disordered energy landscape.[28,29] In our system, excitons are generated with nearly equal probability at any energy site in the QD ensemble (Figure 2a). Over time, the exciton moves energetically downhill due to energy transfer from higher-energy sites to lower-energy sites. The thermalized exciton reaches a final average energy that is determined by site energy disorder and the available thermal energy in the system.[30,31]

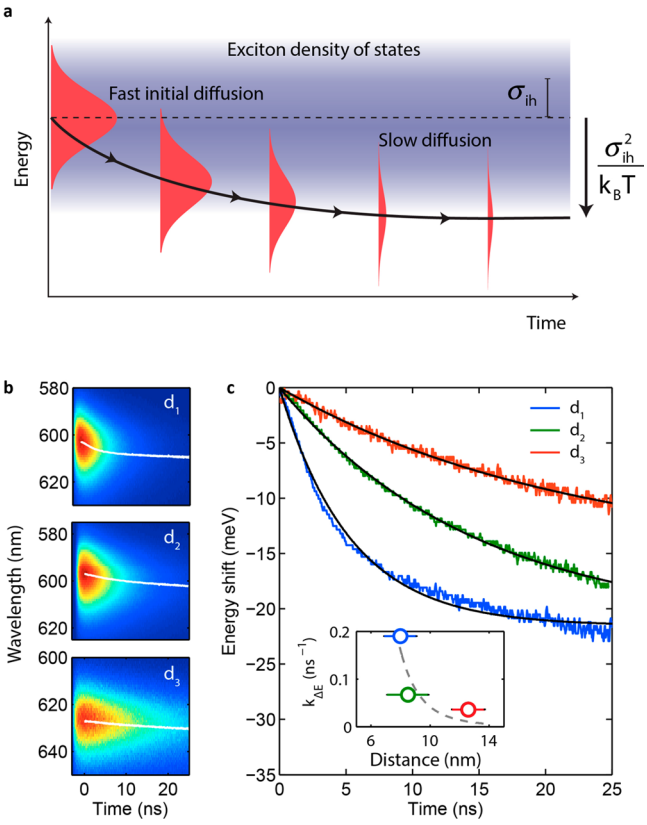

Figure 2. Dynamics of QD emission spectrum. (a) Transient shift of a noninteracting exciton population toward occupation of lower-energy sites within an inhomogeneously broadened ensemble. (b) Spectrally resolved transient photoluminescence collected from the three samples. The linear color scale represents photoluminescence intensity. Solid white markers depict the median emission wavelength as a function of time. (c) Transient red shift of the median emission energy. Solid black lines are fits to the form $\Delta E = \Delta E_{\infty}[1 - \exp(-k_{\Delta E}t)]$. Inset: rate of red shift plotted as a function of QD center-to-center spacing. The dotted line shows $1/d^6$ scaling.

QD materials are known to have energetic disorder arising from variation in QD size within the ensemble.[16,17] To characterize this aspect of our material system, we performed spectrally resolved transient photoluminescence measurements of exciton dynamics. The temporal evolution of the photoluminescence spectrum for the three QD samples is shown in Figure 2b. In all three samples, the median emission energy red shifts with time. These transient red shifts are absent in solution (Supporting Information Figure S12), where QDs are spaced too far apart for excitonic energy transfer to occur. The time-dependent shift of the peak relative to its initial position is plotted in Figure 2C. Solid lines are fits to the form $\Delta E = \Delta E_{\infty}[1 - \exp(-k_{\Delta E}t)]$.[25] The fastest rate of red shifting is observed in samples exhibiting the smallest center-to-center QD spacing. We note that the red shift also causes some broadening of the point-spread function in the spatial measurements, but this effect is within the stated experimental uncertainty (see Supporting Information).

The dynamic red shift is direct evidence of energetic disorder in these QD materials. Bassler[30] showed that for hopping transport within a Gaussian distribution of site energies the median occupied energy saturates at long time to a value

$$\Delta E_{\infty} = -\frac{\sigma_{ih}^2}{k_BT} \quad (3)$$

where σ_{ih} is the width of the inhomogeneous distribution of site energies, and $k_BT = 25$ meV is the thermal energy per degree of freedom at room temperature. The energy shift is determined by a balance between the width of the density of states and thermal excitation out of the lowest energy states. While eq 3 is strictly valid only for hopping processes governed by Boltzmann statistics, it provides a way to estimate the site energy disorder within our QD solids.[32] For samples d_1, d_2, and d_3, we calculate inhomogeneous broadening (reported as fwhm $= 2(2 \ln 2)^{1/2}\sigma_{ih}$) of 54 (±5) meV, 54 (±5) meV, and 47 (±5) meV, respectively. The corresponding homogeneous line widths (fwhm) are then 70 (±7) meV, 68 (±7) meV, and 63 (±7) meV, which is in agreement with recent measurements of similar materials.[33]

The parameter $k_{\Delta E}$, which describes the rate of energy relaxation, is a key indicator of the mechanism of exciton transport in these materials. The rate at which the exciton population approaches a thermalized energy distribution is determined by the site sampling frequency (i.e., how quickly excitons can sample different sites within the ensemble), which is proportional to the average energy transfer rate between neighboring QDs. The exponential decay constant $k_{\Delta E}$ obtained from analysis of the data in Figure 2c is plotted in the inset as a function of QD center-to-center distance. QD materials with smaller interparticle spacing enable faster energy transfer rates. The dotted line shows $1/d^6$ scaling, as expected for energy transfer dominated by dipole−dipole interactions,[34] though we cannot rule out the contribution of higher-order multipoles.[35] These observations, taken together with the bright and long-lived photoluminescence,[14,36] the difficulty of electron tunneling through the inorganic shells and insulating ligands used here,[14,37] previous claims by others,[16,17,22,23] and consistency between experimental observations and numerical simulations (see below) strongly suggest that excitonic energy transfer, and not free charge carrier motion, is responsible for exciton transport in our samples.

If energetic disorder is the origin of subdiffusive transport, then excitons of different energy should have different diffusivities. In Figure 3a, we show spatially resolved measure-

dx.doi.org/10.1021/nl501190s | Nano Lett. 2014, 14, 3556−3562

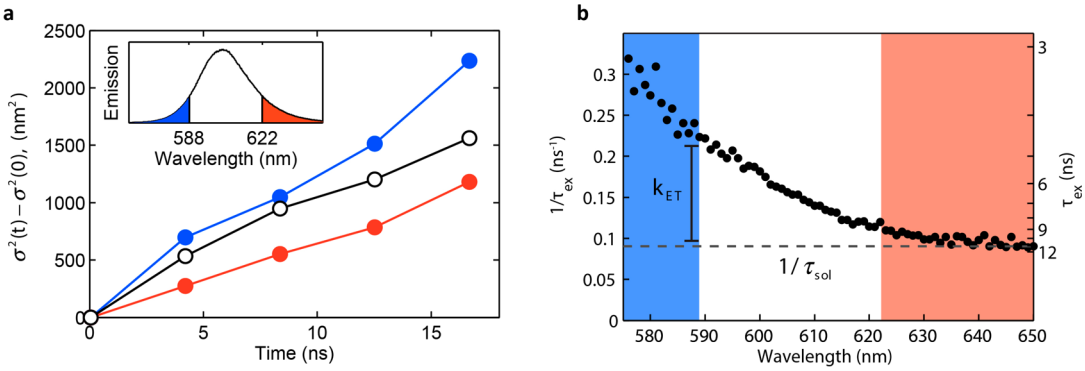

Figure 3. Spectrally resolved exciton transport. (a) Spectrally resolved change in variance, σ^2, of the exciton distribution as a function of time for sample d_1. The inset shows the corresponding wavelength regions of the emission spectrum for the red and blue curves. The black curve represents the spectrally integrated change in variance. (b) Inverse exciton lifetime plotted versus emission wavelength for the same sample. The horizontal dotted line represents the solution-phase lifetime of these QDs. Blue and red colored regions represent the spectral regions depicted in panel a.

ments of exciton transport in three spectral regions. Diffusion is faster for excitons in the higher energy portion of the inhomogeneous distribution than excitons near the bottom of the distribution. Excitons at high energy sites within the sample have larger cumulative hopping rates due to greater probability of finding a lower-energy acceptor nearby. This is confirmed by measuring the exciton lifetime as a function of exciton energy (Figure 3b). The highest-energy excitons have the shortest lifetime (fastest energy transfer rate), whereas the lifetime of low-energy excitons approaches the lifetime of isolated QDs, as measured in solution.

To determine the exciton diffusion length, L_D, in each of these materials we plot the fraction of excitons surviving to some time t versus the net spatial displacement (in one dimension) during that time (see Figure 4a). The curves shown in Figure 4a are generated from the power law fit to the measured exciton spatial distribution (Figure 1d) and the ensemble population decay (Supporting Information Figure S5). The net spatial displacement at a given time is obtained from $L = (\sigma^2(t) - \sigma^2(0))^{1/2}$. By convention, we define the exciton diffusion length, L_D, as the minimum net displacement in one dimension achieved by 37% (i.e., $1/e$) of the exciton population. Exciton diffusion lengths for samples d_1, d_2, and d_3 are found to be 32, 25, and 21 nm, respectively, demonstrating the ability to tune L_D through QD spacing. These values are 2–5 times larger than typical singlet exciton diffusion lengths in organic molecular thin films.[38]

In addition to the effect of QD spacing on exciton diffusion length, our measurements also reveal the influential role played by energetic disorder. Because of a limited exciton lifetime (10–20 ns in these materials), each exciton spends the majority of its lifetime in the transient approach to thermal equilibrium (see Figure 2c). This behavior is in contrast to charge transport systems where thermal equilibrium is reached early in the lifetime of the charge carrier.[30] Consequently, a large fraction of the exciton diffusion length is covered during the first few nanoseconds following photoexcitation, when the exciton population is large and the diffusivity is greatest. The effect of this initial rapid diffusion on the overall exciton diffusion length, L_D, is demonstrated in Figure 4b. The dashed curve in Figure 4b is a hypothetical case of normal diffusion for sample d_1 assuming a constant limiting diffusivity of $D(t \sim 50\ \text{ns}) = 3 \times 10^{-4}$ cm^2/s. Comparing it to the measured (solid) curve for d_1, we see that the initial rapid phase of transport leads to an exciton diffusion length that is 50% larger than one would

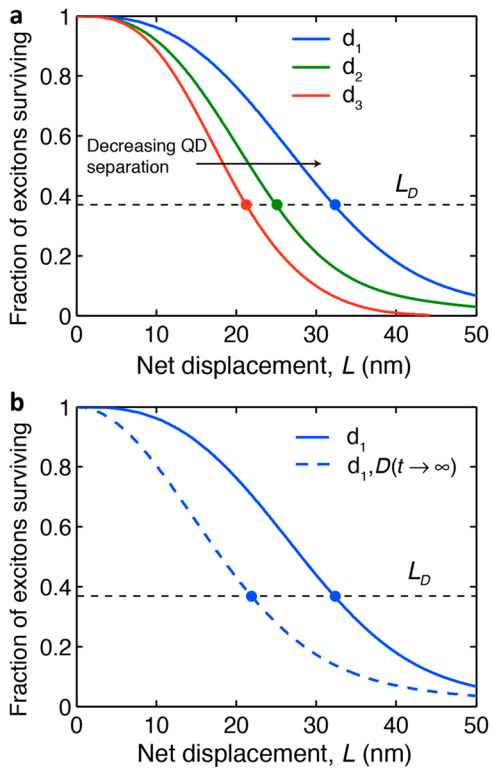

Figure 4. Distribution of exciton propagation lengths. (a) Fraction of excitons that have at least the indicated one-dimensional spatial displacement within their lifetime. The diffusion length, L_D, is determined by the minimum net displacement achieved by 37% (i.e., $1/e$) of the exciton population. (b) Effect of time-dependent (experimentally measured) and constant (hypothetical) diffusivity on exciton diffusion length, assuming a constant limiting diffusivity of $D(t \sim 50\ \text{ns}) = 3 \times 10^{-4}$ cm^2/s.

expect assuming thermalized exciton diffusivity. This result shows that the initial transient approach to a thermalized population defines much of the length scale of exciton transport in disordered systems and should not be neglected when modeling hopping-type exciton transport.[29] In particular, the initial rapid transport contributes significantly to the exciton diffusion length when the rate of energy relaxation ($k_{\Delta E}$) is slow relative to the exciton decay rate ($1/\tau_{ex}$).

To gain insight into the relationship between energetic disorder and the spatiotemporal dynamics of excitons, we

dx.doi.org/10.1021/nl501190s | Nano Lett. 2014, 14, 3556–3562

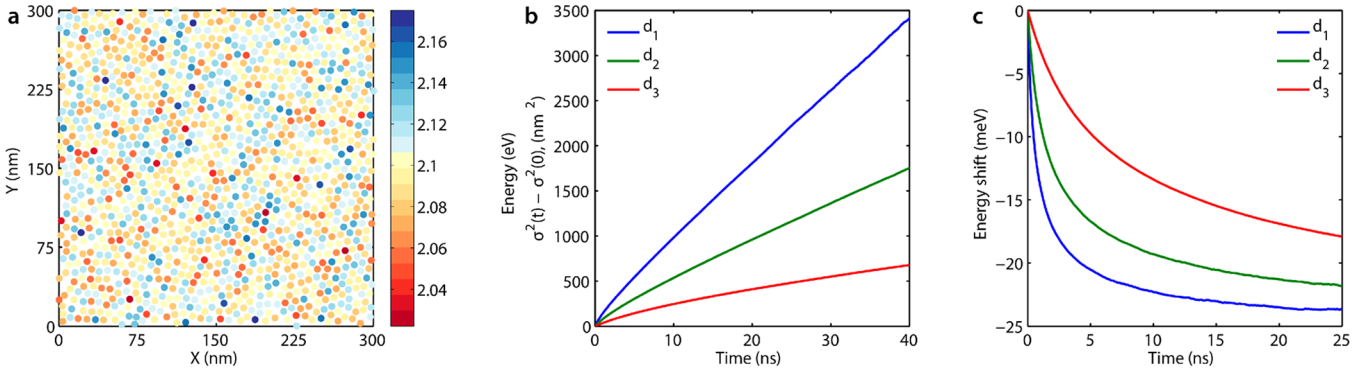

Figure 5. Kinetic Monte Carlo simulations of exciton diffusion. (a) A configuration of a two-dimensional model QD film. Point positions and colors represent the Cartesian coordinate of individual QDs and their absorption peak energies, respectively. (b) Mean-square-displacement as a function of time shown for each simulated QD system. (c) Average transient exciton energy shown for each simulated QD system.

performed kinetic Monte Carlo simulations of exciton transport in a disordered model QD film (see Figure 5a and Supporting Information). We find that a model in which excitons hop between energetically (and spatially) disordered QDs with transition rates determined using Förster theory is capable of reproducing the experimental trends in both exciton displacement (Figure 5b) and transient energetics (Figure 5c). Consistent with experimental observations, the simulations show that increasing the inter-QD separation decreases the diffusion length, reduces the rate of downhill energy migration, and exaggerates the extent of subdiffusivity. Our simulations along with previous theoretical findings[19,30] illustrate that the inclusion of early time nonequilibrium dynamics is required in order to correctly reproduce the experimental observation of time-dependent diffusivity and transient red shift. Figure 6

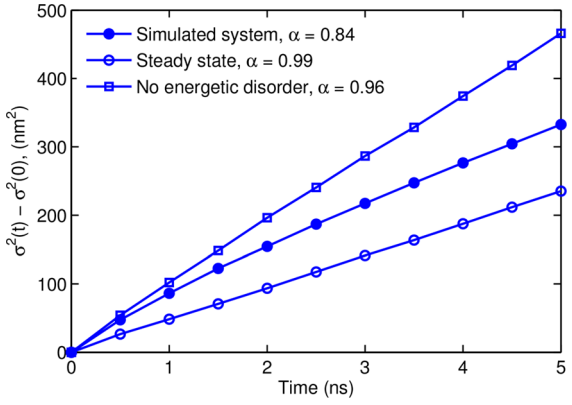

Figure 6. Limiting cases for exciton diffusion. Simulated mean-squared displacement for the d_1 system calculated for excitons in the full simulated system (closed circles, same as in Figure 5b) for excitons initialized with a thermalized steady-state distribution of energies (open circles) or in the absence of energetic disorder (open squares). For each curve, the reported value of α represents a best fit to eq 2.

shows the results of simulations performed in the presence and absence of energetic disorder between QDs and also for the disordered case under conditions for which the initial energetic distribution of excitons is that of the thermalized long time steady state. Unlike the subdiffusive behavior for the full simulated system ($\alpha < 1$), transport follows normal diffusion ($\alpha \approx 1$) both for excitons in the absence of energetic disorder and for thermalized excitons in the presence of energetic disorder, although the effective rate of diffusion is significantly larger in the former case than in the latter. For the full system (nonthermalized excitons with energetic disorder), the diffusivity transitions between that of the energetically uniform system at very short times to that of the energetically disordered but thermalized system at longer times. This highlights the importance of using full kinetic models such as KMC when modeling exciton transport in QD solids.

We have shown that energetic disorder and QD center-to-center distance are important factors in determining exciton diffusion length in QD materials. Additionally, photoluminescence quantum efficiency and emission wavelength (i.e., band gap) are expected to strongly influence exciton diffusion length. For a random walk of dipole-mediated energy transfer events,[39] L_D scales as $\lambda^{5/2}$ due to increased spatial extent of the optical near-field. In a film of near-infrared ($\lambda \approx 1200$ nm) emitting QDs with similar polydispersity, size, and photoluminescence quantum efficiency to our sample d_1, exciton diffusion lengths exceeding 150 nm could be expected. The flexibility in tuning exciton transport without altering luminescent properties allows the rational engineering of QD materials for a particular device application. For example, in excitonic solar cells where a long diffusion length is desired, QDs with a thin shell (or no shell), short ligand, long exciton lifetime, and minimal inhomogeneous broadening are desirable. For LEDs and lasers where isolated noninteracting excitons are desired, QDs with thick shells are ideal. This level of excitonic control is unique to colloidal QD materials and highlights a distinct advantage over organic or bulk inorganic semiconductors.

Methods. *Sample Preparation.* All quantum dot (QD) solutions used in this work were provided by QD Vision Inc. and used as received. Samples d_1 and d_2 have the same particle size and composition (4.2 nm CdSe core with <1 nm thick $Zn_{0.5}Cd_{0.5}S$ shell) but have different organic ligand lengths. Sample d_1 is capped with a short aromatic ligand (benzylphosphonic acid), while d_2 is capped with a long aliphatic ligand (octadecylphosphonic acid). Sample d_3 has a thicker shell (2−3 nm thick) and is capped with a long aliphatic ligand (oleic acid). See the online Supporting Information for detailed characterization.

Glass substrates were cleaned, treated with oxygen plasma, and incubated overnight under inert atmosphere in 2 mM mercaptopropyl trimethoxysilane to form a self-assembled monolayer. Treated samples were subsequently ultrasonicated to remove unbound reagent and returned to a glovebox for spin-casting with 40 mg/mL solutions of each type of QD. The resulting QD solids were approximately 80 nm thick, as

dx.doi.org/10.1021/nl501190s | *Nano Lett.* 2014, 14, 3556−3562

measured by atomic force microscopy, corresponding to ∼6−10 QD layers. To avoid sample oxidation during subsequent measurements in air, each freshly prepared slide was packaged under inert atmosphere by sealing it face-down to a larger cleaned glass slide with two-component epoxy, which was allowed to fully harden in the glovebox before exposure to air.

Time-Resolved Microscopy. Exciton transport in quantum dot films was measured using a custom-built fluorescence microscope. The laser excitation source was a Ti:sapphire ultrafast laser producing pulses ∼100 fs in duration with a reduced repetition rate of 20 MHz, frequency doubled to a wavelength of 400 nm. The beam was filtered by a single mode optical fiber to produce a collimated diffraction limited beam. The single mode beam was directed into the back of an inverted optical microscope and reflected into the objective lens by a long pass dichroic mirror with a cutoff wavelength of λ = 415 nm. The 100×, 1.45 NA, oil immersion objective lens focused the laser beam onto the sample through a glass cover slide to a near diffraction limited spot (∼400 nm fwhm). The convolution of this excitation spot with the point spread function (PSF) for emitted photons[26] results in an imaged fluorescence spot ∼480 nm in width. All measurements were done with an incident average power on the sample of 5 nW at a repetition rate of 20 MHz, corresponding to a pulse energy of 0.25 fJ and a fluence of 0.2 μJ/cm^2. Epi-fluorescence from the sample was collected by the same objective, filtered by a λ = 416 nm cutoff long pass filter, then reimaged by an f = 1000 mm focal length achromatic lens. A single photon detecting avalanche photodiode (APD) with 50 μm active area was mounted in the focal plane on a two-dimensional computer-controlled translation stage, and the APD signal was fed to a time-correlated single-photon counting module. The APD active area was scanned with a velocity of 2.5 μm/s across the magnified fluorescence image, generating time-resolved fluorescence intensity data at each position within the image plane. The overall instrument response function was ∼30 ps. Each measurement had a duration of 30 min during which the sample was scanned in the XY plane to average out any inhomogeneity in the film and to avoid photobleaching. No focus drift was observed during the measurement.

The choice of film thickness (in this case, ∼80 nm) is unimportant as long as the film is substantially thicker than a monolayer of QDs (8−12 nm). Importantly, the measurement is not affected by exciton diffusion in the surface-normal direction (z-direction) or by the optical absorption length. Since hopping rates in all directions are independent, diffusion in the surface-normal (z) direction does not affect the measured diffusivity in the x−y plane. As implemented, the measurement technique integrates all exciton density in the surface-normal direction, so that analysis reduces to a two-dimensional problem (if the variance is calculated by spatial integration of 2D data) or a one-dimensional problem (if the variance is calculated by spatial integration of a 1D cross-section of the time-dependent distribution, as we have done). We note that the actual 3D displacement of the exciton is larger than our reported values by a factor $\sqrt{3}$, but we have used the convention in the literature of reporting diffusion length in one dimension, as this is the relevant length scale for device design.

Spectrally Resolved Transient Photoluminescence. Spectrally resolved transient photoluminescence of the quantum dot films was measured using a custom-built fluorescence microscope, similar to the instrument used for time-resolved microscopy. The laser excitation source was a 405 nm laser diode producing pulses ∼500 ps in duration with a repetition rate of 10 MHz. A 60×, 1.4 NA, oil immersion objective lens focused the laser beam and collected epi-fluorescence. The collimated fluorescence beam was focused into a 0.5 m focal length spectrograph, diffracted by an 800 nm blaze grating, and spectrally filtered by the exit slit. A spectral line 1 nm in width was focused onto an APD, which was connected to a timing module. The spectrograph grating was scanned across the spectral range of interest at 1 nm intervals, while recording time-resolved fluorescence intensity at each wavelength, thereby generating a map of spectrally resolved fluorescence intensity as a function of time.

Kinetic Monte Carlo Simulations. The dynamics of individual excitons were simulated numerically using a kinetic Monte Carlo (KMC) algorithm in which a single exciton undergoes a series of stochastic hops between individual quantum dots (QDs). The model system consisted of a single spatially disordered configuration of 2500 model QDs in a two-dimensional periodically replicated simulation cell (see Figure 5a and Supporting Information). Each QD was randomly assigned a fixed transition dipole vector, $\hat{\mu}$, and absorption energy, ε, the former distributed uniformly on the surface of a unit sphere and the latter drawn from a Gaussian distribution

$$P(\varepsilon) = \frac{1}{\sigma_{\mathrm{ih}}\sqrt{2\pi}} \exp\left[-\frac{(\varepsilon - \varepsilon_{\mathrm{peak}})^2}{2\sigma_{\mathrm{ih}}^2}\right] \tag{4}$$

where σ_{ih} represents the inhomogeneous broadening and $\varepsilon_{\mathrm{peak}}$ is the energy at the peak of the first absorption feature. The transition probability per unit time, $k_{i\to j}$, for an exciton to move from the ith to the jth QD is given by the Förster rate equation

$$k_{i\to j} = \frac{1}{\tau}\left(\frac{R_0}{d_{ij}}\right)^6 \tag{5}$$

where τ is the experimentally determined exciton lifetime, R_0 is the Förster radius (determined by the spectral overlap between each pair of QDs—see Supporting Information) and d_{ij} is the distance between QDs i and j. In addition to hopping, excitons undergo decay with a rate equal to τ^{-1}. A more detailed description of the numerical simulation is included in the Supporting Information.

■ ASSOCIATED CONTENT

Ⓢ Supporting Information

Further details on the materials and methods. This material is available free of charge via the Internet at http://pubs.acs.org.

■ AUTHOR INFORMATION

Corresponding Author

*E-mail: tisdale@mit.edu.

Author Contributions

G.M.A. and F.P. performed and analyzed the spatial diffusion measurements. F.P. and L.V.P. prepared the samples and performed and analyzed the transient spectroscopy measurements. E.M.Y.L. assisted in the interpretation of the spatial diffusion data and together with A.P.W. performed the KMC simulations. M.C.W. performed and analyzed the electron microscopy. A.J.M. assisted in sample preparation and in the transient spectroscopy measurements. G.M.A., F.P., and W.A.T. conceived and designed the experiments and wrote the manuscript. V.B. and W.A.T. supervised the project. All authors

contributed to the interpretation of data and assisted in the manuscript preparation.

Author Contributions

[#]G.M.A. and F.P. contributed equally to this work.

Notes

The authors declare no competing financial interest.

■ ACKNOWLEDGMENTS

The authors thank Parag Deotare for key contributions to the development of the exciton diffusion imaging technique and insightful discussions. This work was supported as part of the Center for Excitonics, an Energy Frontier Research Center funded by the U.S. Department of Energy, Office of Science, Office of Basic Energy Sciences under award no. DE-SC0001088 (MIT). Exciton diffusion imaging measurements were performed in the MIT Nanostructured Materials Metrology Laboratory within the MIT Center for Materials Science and Engineering on equipment provided by the Eni-MIT Solar Frontiers Center. G.M.A. acknowledges support from the Hertz Foundation Fellowship. G.M.A., E.M.Y.L., M.C.W., and A.J.M. acknowledge partial support from the National Science Foundation Graduate Research Fellowship Program under Grant 1122374. We thank Jonathan Steckel and Seth Coe-Sullivan of QD Vision, Inc., for supplying QD materials.

■ REFERENCES

(1) Alivisatos, A. *Science* **1996**, *271*, 933−937.
(2) Graetzel, M.; Janssen, R. A. J.; Mitzi, D. B.; Sargent, E. H. *Nature* **2012**, *488*, 304−312.
(3) Shirasaki, Y.; Supran, G.; Bawendi, M.; Bulović, V. *Nat. Photonics* **2012**, *7*, 13−23.
(4) Semonin, O. E.; Luther, J. M.; Choi, S.; Chen, H.-Y.; Gao, J.; Nozik, A. J.; Beard, M. C. *Science* **2011**, *334*, 1530−1533.
(5) Tisdale, W. A.; Williams, K. J.; Timp, B. A.; Norris, D. J.; Aydil, E. S.; Zhu, X.-Y. *Science* **2010**, *328*, 1543−1547.
(6) Mashford, B.; Stevenson, M.; Popovic, Z.; Hamilton, C.; Zhou, Z.; Breen, C.; Steckel, J.; Bulović, V.; Bawendi, M. G.; Coe-Sullivan, S.; Kazlas, P. T. *Nat. Photonics* **2013**, *7*, 407−412.
(7) Ip, A. H.; Thon, S. M.; Hoogland, S.; Voznyy, O.; Zhitomirsky, D.; Debnath, R.; Levina, L.; Rollny, L. R.; Carey, G. H.; Fischer, A.; Kemp, K. W.; Kramer, I. J.; Ning, Z.; Labelle, A. J.; Chou, K. W.; Amassian, A.; Sargent, E. H. *Nat. Nanotechnol.* **2012**, *7*, 577−582.
(8) Konstantatos, G.; Howard, I.; Fischer, A.; Hoogland, S.; Clifford, J.; Klem, E.; Levina, L.; Sargent, E. H. *Nature* **2006**, *442*, 180−183.
(9) Konstantatos, G.; Badioli, M.; Gaudreau, L.; Osmond, J.; Bernechea, M.; de Arquer, F. P. G.; Gatti, F.; Koppens, F. H. L. *Nat. Nanotechnol.* **2012**, *7*, 363−368.
(10) Klimov, V. I.; Ivanov, S. A.; Nanda, J.; Achermann, M.; Bezel, I.; Mcguire, J. A.; Piryatinski, A. *Nature* **2007**, *447*, 441−446.
(11) Dang, C.; Lee, J.; Breen, C.; Steckel, J. S.; Coe-Sullivan, S.; Nurmikko, A. *Nat. Nanotechnol.* **2012**, *7*, 335−339.
(12) Sun, L.; Choi, J. J.; Stachnik, D.; Bartnik, A. C.; Hyun, B.-R.; Malliaras, G. G.; Hanrath, T.; Wise, F. W. *Nat. Nanotechnol.* **2012**, *7*, 369−373.
(13) Talgorn, E.; Gao, Y.; Aerts, M.; Kunneman, L. T.; Schins, J. M.; Savenije, T. J.; van Huis, M. a; van der Zant, H. S. J.; Houtepen, A. J.; Siebbeles, L. D. A. *Nat. Nanotechnol.* **2011**, *6*, 733−739.
(14) Choi, J. J.; Luria, J.; Hyun, B.-R.; Bartnik, A. C.; Sun, L.; Lim, Y.-F.; Marohn, J. A.; Wise, F. W.; Hanrath, T. *Nano Lett.* **2010**, *10*, 1805−1811.
(15) Lee, J.-S.; Kovalenko, M. V.; Huang, J.; Chung, D. S.; Talapin, D. V. *Nat. Nanotechnol.* **2011**, *6*, 348−352.
(16) Kagan, C.; Murray, C.; Bawendi, M. *Phys. Rev. B* **1996**, *54*, 8633−8643.
(17) Crooker, S.; Hollingsworth, J.; Tretiak, S.; Klimov, V. *Phys. Rev. Lett.* **2002**, *89*, 186802.
(18) Zhitomirsky, D.; Voznyy, O.; Hoogland, S.; Sargent, E. H. *ACS Nano* **2013**, *7*, 5282−5290.
(19) Gao, Y.; Suchand Sandeep, C. S.; Schins, J. M.; Houtepen, A. J.; Siebbeles, L. D. A. *Nat. Commun.* **2013**, *4*, 2329.
(20) Gao, Y.; Talgorn, E.; Aerts, M.; Trinh, M. T.; Schins, J. M.; Houtepen, A. J.; Siebbeles, L. D. A. *Nano Lett.* **2011**, *11*, 5471−5476.
(21) Moroz, P.; Kholmicheva, N.; Mellott, B.; Liyanage, G.; Rijal, U.; Bastola, E.; Huband, K.; Khon, E.; McBride, K.; Zamkov, M. *ACS Nano* **2013**, *7*, 6964−6977.
(22) Achermann, M.; Petruska, M. A.; Crooker, S. A.; Klimov, V. I. *J. Phys. Chem. B* **2003**, *107*, 13782−13787.
(23) Miyazaki, J.; Kinoshita, S. *Phys. Rev. B* **2012**, *86*, 035303.
(24) Xu, F.; Ma, X.; Haughn, C.; Benavides, J. *ACS Nano* **2011**, *5*, 9950−9957.
(25) Poulikakos, L. V.; Prins, F.; Tisdale, W. A. *J. Phys. Chem. C* **2014**, *118*, 7894−7900.
(26) Akselrod, G. M.; Deotare, P. B.; Thompson, N. J.; Lee, J.; Tisdale, W. A.; Baldo, M. A.; Menon, V. M.; Bulovic, V. *Nat. Commun.* **2014**, *5*, 3646.
(27) Song, C.; Wang, P.; Makse, H. A. *Nature* **2008**, *453*, 629−632.
(28) Bouchaud, J.-P.; Georges, A. *Phys. Rep.* **1990**, *195*, 127−293.
(29) Ahn, T.-S.; Wright, N.; Bardeen, C. J. *Chem. Phys. Lett.* **2007**, *446*, 43−48.
(30) Bassler, H. *Phys. Status Solidi* **1993**, *175*, 15−56.
(31) Fennel, F.; Lochbrunner, S. *Phys. Rev. B* **2012**, *85*, 094203.
(32) Madigan, C.; Bulović, V. *Phys. Rev. Lett.* **2006**, *96*, 046404.
(33) Cui, J.; Beyler, A. P.; Marshall, L. F.; Chen, O.; Harris, D. K.; Wanger, D. D.; Brokmann, X.; Bawendi, M. G. *Nat. Chem.* **2013**, *5*, 602−606.
(34) Swenberg, C.; Pope, M. *Electronic Processes in Organic Crystals and Polymers*; Oxford University Press: New York, 1999.
(35) Baer, R.; Rabani, E. *J. Chem. Phys.* **2008**, *128*, 184710.
(36) Wanger, D. D.; Correa, R. E.; Dauler, E. A.; Bawendi, M. G. *Nano Lett.* **2013**, *13*, 5907−5912.
(37) Yu, D.; Wang, C.; Guyot-Sionnest, P. *Science* **2003**, *300*, 1277−1280.
(38) Lunt, R. R.; Giebink, N. C.; Belak, A. A.; Benziger, J. B.; Forrest, S. R. *J. Appl. Phys.* **2009**, *105*, 53711.
(39) Menke, S. M.; Luhman, W. A.; Holmes, R. J. *Nat. Mater.* **2013**, *12*, 152−157.